Testing the MCS Deconvolution Algorithm on Infrared Data

Michael P. Egan
National Geospatial-Intelligence Agency
Basic and Applied Research Office

ABSTRACT

Magain, Courbin, and Sohy (MCS, 1998) [1] proposed a two-channel (separable point source plus extended background) method for astronomical image deconvolution. Unlike the two-channel Richardson-Lucy algorithm [2], [3], the MCS method does not require prior knowledge of point source amplitudes and positions. MCS claim that their method produces accurate astrometry and photometry in crowded fields and in the presence of variable backgrounds. This paper compares Midcourse Space Experiment (MSX) 8 μm Galactic plane images [4] deconvolved via the MCS method to Spitzer Space Telescope Glimpse Survey [5] 8 μm images of the same fields. The improved sampling and final image point spread function (PSF) for the deconvolved MSX image is chosen to match the Spitzer observation. In the parlance of MCS, this determines the light distribution from an 85 cm telescope (Spitzer) by deconvolving data taken with a 33 cm space telescope (MSX). Results are presented for varying degrees of background complexity and examine the limitations of the MCS method for use on infrared data in regions of high source density and bright complex backgrounds.

1.   DECONVOLUTION WITH CORRECT SAMPLING

Starck, Pantin, and Murtagh [6] in their 2002 review of deconvolution methods define super resolution as "recovering object spatial frequency information outside the spatial bandwidth of the image formation system." Their review of the theoretical literature admits that true super-resolution is possible if the object to be resolved is nearly black – that is, most pixels in the data have zero values and the non-zero elements are well-spaced [7]. This is certainly true in many astronomical images, though it leads to difficulties in areas with structured backgrounds. While true super-resolution is not possible for extended objects that are not band-limited, the super-resolution techniques will provide image sharpening and contrast enhancement. [8]

We may write the observed distribution of light from a source, $d(x)$, as measured by a given instrument, as

$$d(\mathbf{x}) = p(\mathbf{x}) * f(\mathbf{x}) + n(\mathbf{x})$$

where $p(x)$ is the total system point response function (PRF), $f(x)$ is the true light distribution, and $n(x)$ is the noise inherent in the measured data. Deconvolution is the effort to remove the effect of the point response function, and our recovery of the higher spatial resolution image consistent with the true light distribution yields a super-resolution image.

Typical deconvolution algorithms seek to minimize the function

$$S = \sum_{i=1}^{N} \frac{1}{\sigma_i^2} \left[\sum_{j=1}^{N} t_{ij} f_j - d_i \right]^2 + \lambda H(\mathbf{f})$$

where the first term is a χ^2 function formed by the difference between the modeled true image, $t(x)*f(x)$ and the measured data $d(x)$. In astronomical imaging, the solution, $f(x)$, in many deconvolution algorithms is assumed to be a sum of delta functions on a flat background. In many deconvolution algorithms, bandwidth limiting by the detector system of higher spatial frequencies plus the presence of noise often result in ringing, spurious sources, and lack of flux conservation for direct deconvolution techniques.

The second term in the above equation – the regularization function - contains a Lagrange multiplier, λ, and a smoothing function, *H(f)*. The smoothing term can generally be thought of as a constraint on the reconstructed image, and the form it takes drives the nature of the solution. Unconstrained, the solution to the inverse problem has a variety of plausible solutions; the regularization function provides a criterion to determine a stable and unique solution. [7] Many regularization methods, such as Maximum Entropy, and maximum likelihood are global constraints. While these can solve some of the ringing artifacts, they are problematic in that they mathematically couple regions in the solution that are clearly not physically related. This manifests itself in photometric errors in the deconvolution solution and in serving to smooth sources that should be sharp.

More recent developments in deconvolution algorithms have found that local constraints on the smoothness of the background are more effective in reducing reconstruction artifacts than global constraints. Other work has shown that modeling point source components of an image separately from the extended background can result in superior performance of super-resolution imaging algorithms. These "two channel" methods – model the form of the true light distribution as *f(x)* + *h(x)*, where *f(x)* is made up of the point sources in the observed field, and *h(x)* is the extended component of the light distribution.

Magain, Courbin, and Sohy [1] have defined a two-channel deconvolution algorithm that avoids the ringing artifacts seen in some deconvolution algorithms. MCS shares characteristics with both the CLEAN algorithm and the two-channel Richardson-Lucy algorithm [6], but differs from these in that the point source components are not modeled as delta functions. The MCS algorithm is based on the principle that sampled data cannot be fully deconvolved, i.e. yielding delta function-type point sources, without violating the sampling theorem.

The MCS technique seeks to minimize the function

$$S_2 = \sum_{i=1}^{N} \frac{1}{\sigma_i^2} \left[\sum_{j=1}^{N} s_{ij} \left(h_j + \sum_{k=1}^{M} a_k r(x_j - c_k) \right) - d_i \right]^2 + \lambda \sum_{i=1}^{N} \left(h_i - \sum_{j=1}^{N} r_{ij} h_j \right)^2$$

where the point response function (PRF) of the original imaging system is represented by

$$p(x) = r(x) * s(x).$$

In the above equation the original data PRF, *p(x)* is assumed to be reproducible by the convolution of the PRF of the "ideal" system, *r(x)*, and the "deconvolution kernel" *s(x)*. The "ideal" system defines the resolution, and the image sampling needed for the super-resolution image. In practice, since *p(x)* is known, and *r(x)* is defined by the user, the deconvolution kernel, *s(x)* is solved for from these. Instead of a global technique, MCS opts for a regularization function that imposes local smoothness of the background component on the length scale of the PSF of the solution, *r(x)*.

Noise limits the degree to which image data can be deconvolved and reconstructed at super-resolution length scales. Beyond photon noise, infrared detectors often exhibit image artifacts, particularly at the high gain and low background settings used for astronomical imaging. These artifacts are typically associated with bright sources and result in pattern noise along rows or columns. The model solution, f*(x)* + h*(x)*, does not account for noise, but it is of course inherent in the data. Therefore, the noise and its form will affect the final results. How well MCS can reconstruct images in the presence of noise is of interest to this preliminary study.

2. COMPARISON OF MSX AND SPITZER GALACTIC PLANE DATA

Price et al (2001) [4] describe the MSX Galactic Plane Survey and the SPIRIT III Telescope in full detail. In brief, the MSX infrared instrument, the SPIRIT III telescope was a cryogenically cooled 33 cm telescope. The infrared arrays had six spectral bands, centered at 4.3, 4.4, 8.28, 12.13, 14.65, and 23.4 microns. The 8.28 μm band, which spanned a spectral range from 6.8 to 11 μm was the most sensitive. In the Galactic plane survey, the detection limit for the catalog was about 150 mJy in the 8.28 μm band, typically representing an SNR of 5 [9].

NASA's Spitzer Space Telescope [10] is the last of the Great Observatory series, and is a cryogenically cooled infrared telescope with an 85 cm primary mirror. In the mid-infrared the imaging instrument is the Infrared Array Camera, IRAC [11] with four passbands, centered at 3.6, 4.5, 5.8, and 8.0 μm. The 8.0 μm bandpass cutoffs are from 6.5 to 9.5 μm. Among a number of Legacy Observation programs, the GLIMPSE survey [5] is conducting an IRAC survey of much of the Galactic plane.

If we measure the resolution possible by both MSX and Spitzer by the Rayleigh criterion, $R = 1.22\lambda/D$, we find that given the long wavelength cutoffs of each instrument, the best resolution possible with the optics of each telescope is ~40 microradians (~8 arcsec) for MSX, and ~12 microradians (2.85 arcsec) for Spitzer. In practice, the angular IFOV of the detector elements also affects the resolution. The detector array pixels on the MSX infrared arrays subtended ~18 arcsec, and the resulting PSF in the 8.0 μm band had a FWHM of 20 arcesec [4], which is the final resolution limit of the MSX images. Spitzer detector pixels subtend 1.2 arcsec, so the theoretical resolution limit is roughly the final image resolution of the system. Figs. 1-4 compare the resolution for two example fields in the Galactic plane from both the MSX Survey and the GLIMPSE survey. Note for the Spitzer data, the image artifacts below and to the right of each of the bright sources. These are known artifacts of the detector array that appear for sources nearing the saturation limit of the detectors.
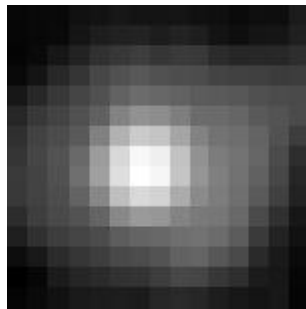

Fig. 1 MSX Image, Galactic coordinates l = 24. 7 b=0.7
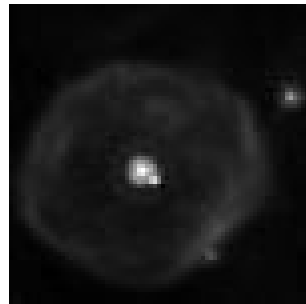

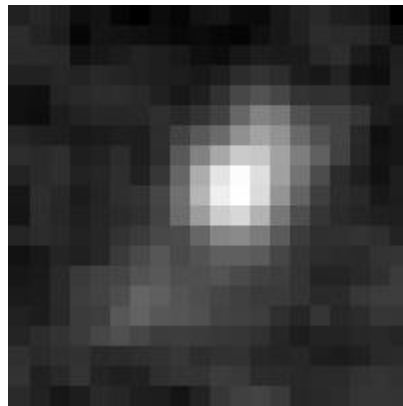**Fig. 2 Spitzer GLIMPSE Image, Galactic coordinates l=24.7 b=0.7**

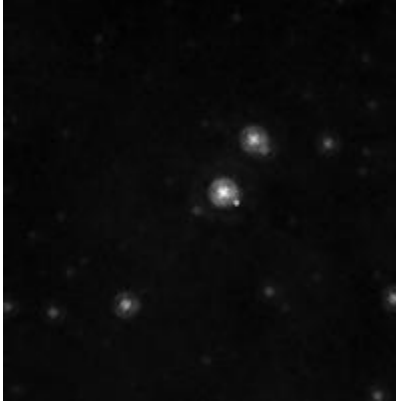**Fig 3 MSX Image, Galactic coordinates l=24.9, b=0.6**

Fig 4 Spitzer GLIMPSE Image, Galactic coordinates l=24.9, b=0.6

3. POINT SOURCE DECONVOLUTION WITH BENIGN BACKGROUND

The simplest test of the deconvolution algorithm is to extract sources against a reasonably flat background, such as that seen in Fig. 2 at the Galactic coordinates l = 24.5798, b=0.6890. The MSX mission catalogued [9] only one source in this field, an 8.3 μm source with intensity 0.542 Jy, at l = 24.5782, b= +0.6901. The higher resolution and greater sensitivity of the SIRTF IRAC instrument resolves this source into two point sources, and also detects many other point sources in the field, the seven brightest of which are listed in Table 1. In the MSX image (Fig 3.) the source appears somewhat elongated from the known PSF, suggesting the presence of a second source. The SIRTF data resolves the sources clearly, and indicates that they are separated by 15.8 arcsec. This is close enough to be resolved by the optics, but beyond the system resolution imposed by the 18 arcsec detectors of the instrument. The MCS algorithm resolves these sources from the data, calculating their separation distance as 17.6 arcsec. In addition, the third brightest point source in the field, at 24.5758, 0.6938 is also resolved by the MCS deconvolution, even though it is at an SNR of about 2 in the MSX data.
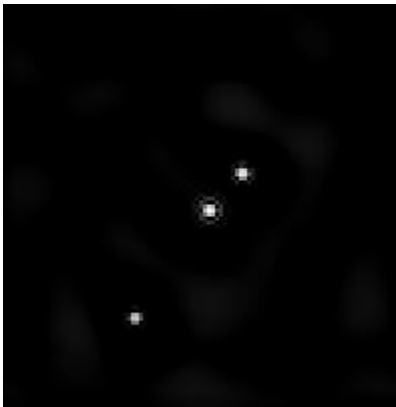

Fig 5 MCS Super-resolution MSX data, Galactic coordinates l=24.9, b=0.6

Table 1 Brightest Point Sources in the l= 24.9, b=0.6 field.

Spitzer Sources			MSX6C Catalog			MCS Extractions		
ℓ (deg)	b (deg)	$F_{Spitzer}$(Jy)	ℓ (deg)	b (deg)	F_{MSX}(Jy)	ℓ (deg)	b (deg)	F_{MCS}(Jy)
24.5783	0.6894	0.5689	24.5782	+0.6901	0.542	24.5793	0.6883	0.520
24.5758	0.6938	0.2405				24.5762	0.6921	0.270
24.5865	0.6801	0.0948				24.5854	0.6796	0.150
24.5641	0.6806	0.0657						
24.5696	0.6935	0.0295						
24.5925	0.6794	0.0018						

4. DECONVOLUTION WITH STRUCTURED BACKGROUND

As with the benign background case, the performance against a structured background by the MCS algorithm was fairly good for point sources, within the limits imposed by the noise inherent in the MSX data. The algorithm did extract the previously extracted high SNR point source, and detected a low SNR source not detected in the MSX6C catalog processing. As before, the flux is overestimated for the low SNR point source. In this case, however, the photometry of the bright source was affected in the reconstruction. The MCS extracted flux density is appreciably less than the MSX or Spitzer catalog brightness. None of the very low SNR point sources seen at the edges of the ring nebula by in the Spitzer IRAC image were extracted or reconstructed by the MCS algorithm.

In terms of reconstructing the extended nebula, we do recover information, including the general rhomboidal shape of the nebula, and the distinction between the low and high brightness regions of the nebula. However, the overall thinness, and the fine structure seen in the high resolution Spitzer image is not recovered by the MCS reconstruction. This is consistent with the theoretical papers, which indicate that for extended objects we can obtain contrast enhancement, but not true superresolution.
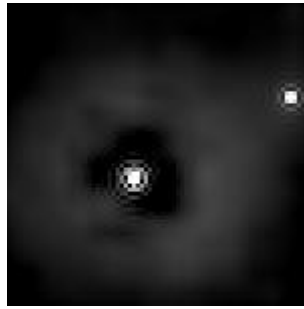

Fig 6 MCS Super-resolution MSX data, Galactic coordinates l=24.7, b=0.7

Table 2 Brightest Point Sources in the l= 24.7, b=0.7 field.

Spitzer Sources			MSX6C Catalog			MCS Extractions		
ℓ (deg)	$\textbf{\textit{b}}$ (deg)	$F_{Spitzer}$(Jy)	ℓ (deg)	$\textbf{\textit{b}}$ (deg)	F_{MSX}(Jy)	ℓ (deg)	$\textbf{\textit{b}}$ (deg)	F_{MCS}(Jy)
24.7288	0.6911	1.537	24.7287	+0.6911	1.964	24.7309	0.6921	0.960
24.7163	0.6973	0.194				24.7136	0.7011	0.214
24.7258	0.713	0.0134						

5. LIMITATIONS OF DECONVOLUTION

The limitations of deconvolution become readily apparent in the MSX scale to Spitzer scale deconvolution. While the MCS method does not introduce ringing, or associated spurious point sources, it is noise limited with respect to the sources that can be identified for image reconstruction. Table 1 lists the point sources extracted by GLIMPSE, MSX, and the deconvolution of the MSX imagery. For MSX, only one source is extracted (at SNR > 2.7) in the 120" x 120" field. While at 8 microns, GLIMPSE detects three sources that might have been detectable by MSX under certain favorable circumstances. The MCS deconvolution does extract these sources from the MSX image, and the position and flux information are consistent with the "truth" data from the Spitzer image. We do see a flux bias in the low SNR sources extracted by the MCS method, consistent with the fact that the combination of positive noise addition to a low SNR source will raise it above the detectability threshold, at the price of a flux bias in the photometry. However, the SNR in the MSX data is ultimately the limiting factor in the recovery of point sources by the MCS deconvolution algorithm.

In reconstructing the extended background, the MCS method does successfully recover point sources and sharpen the extended emission in the original image data. However, SNR limits and the fact that the bulk of the image is no longer "black" hamper the ability to enhance the spatial resolution of the extended ring nebula in our data.

6. CONCLUSIONS

We have demonstrated the utility of the MCS deconvolution algorithm on MSX data, comparing it to truth data taken by the Spitzer IRAC instrument. Super-resolution of point sources and contrast enhancement of extended background components is possible from this data, in spite of the noise artifacts and undersampling of the PRF in the original image data. We have demonstrated that the ultimate limit for deconvolving point sources from the image data is the SNR of a given source in the original data. The technique would be of use in extracting low SNR sources in crowded regions that are missed by standard photometric processing techniques and/or in crowded regions of the sky. Future research will examine the effects of different types of noise artifacts (multiplexer bleed, striping, and other pattern noise) associated with infrared detectors and their effect on limiting the utility of deconvolution algorithms.

7.   REFERENCES

1.   Magain, P., Courbin, F., Sohy, S., Deconvolution with Correct Sampling, *The Astrophysical Journal*, Vol. 494, 472-477, 1998.
2   Richardson, W.H., Bayesian-based iterative method of image restoration, *Journal of the Optical Society of America,* Vol. 62, 745, 197455, 1972.
3   Lucy, L.B., An iterative technique for the rectification of observed distributions, *Astronomical Journal,* Vol. 79, 745, 1974.
4   Price, S.D. et al, MSX Survey of the Galactic Plane, *Astronomical Journal,* Vol. 121, 2819, 2001.
5   Benjamin, R. et al., GLIMPSE. I. An SIRTF Legacy Project to Map the Inner Galaxy, *Publications of the Astronomical Society of the Pacific,* Vol. 115, 953, 2003.
6   Starck, J.L., Pantin, E. and Murtagh, F. Deconvolution in Astronomy: A review, *Publications of the Astronomical Society of the Pacific*, Vol. 114, 1051-1069, 2002.
7   Donoho at el., *Journal of the Royal Statistical Society,* Vol. 54, 41, 1992.
8   Puschmann, K.G. and Kneer, F., On super-resolution in astronomical imaging, *Astronomy & Astrophysics*, Vol 436, 373-378, 2005.
9   Egan et al., *The Midcourse Space Experiment Point Source Catalog Version 2.3 Explanatory Supplement,* AFRL-VS-TR-2003-1589, 2003.
10   Werner, M. et al., The Spitzer Space Telescope Mission, *Astrophysical Journal Supplement,* Vol. 154, 1, 2004.
11   Fazio, G. et al. , The Infrared Array Camera (IRAC) for the Spitzer Space Telescope, *Astrophysical Journal Supplement,* Vol. 154, 10, 2004.